Molecular Inhibition for Selective CO_2 Conversion

Authors: Charles E. Creissen,[1] José Guillermo Rivera de la Cruz,[1] Dilan Karapinar,[1] Dario Taverna,[2] Moritz W. Schreiber,[3] Marc Fontecave[1]*

Affiliations:

[1] *Laboratoire de Chimie des Processus Biologiques, CNRS UMR 8229, Collège de France, Paris, France*

[2] *Institut de Minéralogie et de Physique des Milieux Condensés, UMR 7590 CNRS, Sorbonne Universités, UPMC Univ Paris 06, 4 place Jussieu, 75005 Paris, France*

[3] *Total Research and Technology, Refining and Chemicals, Division CO_2 Conversion, Feluy, 7181 Seneffe, Belgium*

*Corresponding author. Email: marc.fontecave@college-de-france.fr

Abstract:

Electrochemical CO_2 reduction presents a sustainable route to the production of chemicals and fuels. Achieving a narrow product distribution with copper catalysts is challenging and conventional material modifications offer limited control over selectivity. Here, we show that the mild cathodic potentials required to reach high currents in an alkaline gas-fed flow cell permits retention of a surface-bound thiol (4-mercaptopyridine), enabling molecule-directed selective formate generation at high reaction rates. Combined experimental and computational results showed that formate production is favoured due to the inhibition of a CO-producing pathway caused by destabilising interactions with the anchored molecule. The immobilisation of molecules to inhibit specific carbon-based products therefore offers a novel approach to rationally tune the selectivity of heterogeneous catalysts.

Main Text:

Electrochemical CO_2 reduction (CO_2R) demands selective high-rate product generation with low electrical input, which can be facilitated using heterogeneous electrocatalysts.(*1–4*) Cu-based CO_2R catalysts typically generate a wide range of products,(*5*, *6*) as selectivity is limited by similar thermodynamic potentials and competing kinetic pathways.(*7–9*) Catalyst properties such as size, morphology, facet exposure, and density of grain boundaries can be altered to improve product distributions,(*10–14*) but such modifications often modify multiple properties simultaneously and are convoluted by dynamic changes that can occur under working conditions.(*15–17*) A proposed alternative route to control selectivity is through the immobilisation of organic molecules that can interact with surface-bound reaction intermediates to promote or obstruct specific reaction pathways.(*18–20*) These systems would enable the derivation of structure-selectivity relationships, providing opportunities for rational design of modified heterogeneous catalysts. However, examples where organic small molecules are directly anchored on Cu catalysts have been precluded by their propensity for desorption under CO_2R conditions.

For CO_2R, Cu surfaces have been functionalised with molecular catalysts,(*21*) electrodeposited films,(*22–24*) amino acids,(*25*) and polymer-based layers,(*26*, *27*) but covalent immobilisation of distinct small molecules has proven more difficult. Thiols are capable of forming covalent bonds with Cu surfaces but are susceptible to reductive desorption at the high cathodic potentials generally required for CO_2R.(*28*, *29*) This has restricted molecule choice to exclusively long alkyl chains that are retained close to the surface due to their high hydrophobicity.(*30*, *31*) However, recent developments have shown that alkaline gas-fed flow cells are capable of reaching high current densities with low overpotentials.(*32*, *33*) We pursued this beneficial characteristic to understand if reductive desorption of a thiol could be prevented to provide molecular control over CO_2R selectivity. Here, 4-mercaptopyridine (SPy) was immobilised on a Cu catalyst and incorporated in a gas-fed flow cell for high-current density operation (Fig. 1A, Fig. S1).

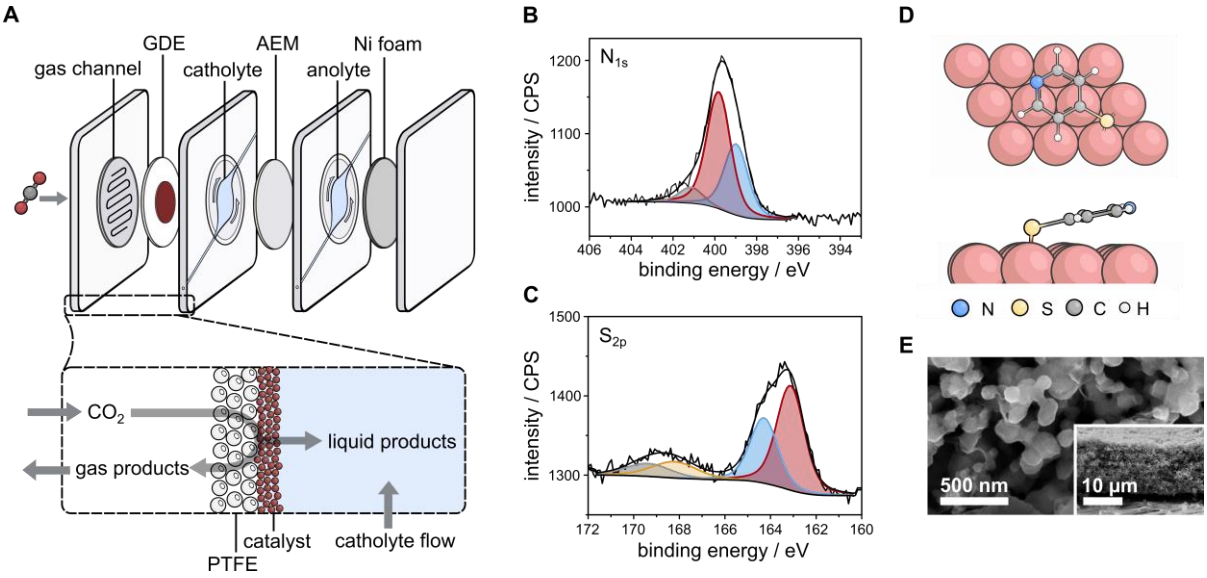

Fig. 1: Thiol functionalisation of Cu and incorporation in a gas-fed flow cell.

(**A**) Schematic of the gas fed flow cell setup and components, in which AEM is an anion exchange membrane and GDE is the gas diffusion electrode. The CO_2 is fed through the back of the PTFE layer via the gas channel. (**B** and **C**) XPS spectra of Cu-SPy powder showing N_{1s} and S_{2p} environments (background and envelope represented by black lines). (**D**) Schematic representation of the most stable configuration of 4-mercaptopyridine (SPy) on Cu as determined using DFT calculations. (**E**) SEM images of the Cu-SPy electrodes.

We immobilised SPy on the surface of Cu nanoparticles (NPs) through self-assembly from organic solution. Successful anchoring was initially confirmed using Fourier-transform infrared (FTIR) spectroscopy, which showed signals corresponding to the surface-bound ligand (Fig. S2). X-ray photoelectron spectroscopy (XPS) was used to further verify SPy attachment (Figs. 1B and 1C, Table S1). The N_{1s} XPS spectrum showed three distinct environments corresponding to protonated and deprotonated forms of SPy,(*34*) and the S_{2p} spectrum showed signals arising from physisorbed thiol (164.3 eV) and covalently-bound thiolate (163.1 eV) sulfur environments, alongside small amounts of residual oxidised sulfur (168.2 & 169.4 eV), as expected for this type of immobilisation procedure.(*35*, *36*) DFT calculations to determine the optimised conformation of SPy showed that the S preferentially binds two Cu atoms with the ring slightly tilted away from the Cu surface (Fig. 1D). We observed no obvious differences in morphology or size between unfunctionalised Cu and Cu-SPy, showing that the

modification does not result in surface restructuration (Fig. S3).(*37*) Gas diffusion electrodes (GDEs) were prepared by airbrushing a methanolic solution of ionomer (Nafion) and functionalised CuNPs onto PTFE membranes to form a porous network (approximately 10 µm thick) (Fig. 1E). A geometrical molecular loading of 15 nmol cm^{-2} was determined by UV-Vis spectroscopy after reductive desorption of SPy at −2.2 V vs. Ag/AgCl/$KCl_{3.4M}$ (Note S1).

We observed that in alkaline conditions (5 M KOH), GDEs could reach −500 mA cm^{-2} at applied potentials of approximately −0.5 V vs. RHE with no significant differences between the current-voltage responses for Cu and Cu-SPy samples (Fig. 2A, Fig. S4). Controlled current electrolysis (CCE) experiments using Cu and Cu-SPy GDEs were conducted at different current densities to see if the molecular species influenced selectivity. Cu-SPy GDEs displayed remarkably high faradaic efficiency (FE) values for $HCOO^-$ of (81 ± 4)% at −100 mA cm^{-2} and (72 ± 2)% at −300 mA cm^{-2} with a maximal partial current density for formate of 217 ± 5 mA cm^{-2} and a corresponding cathodic energy efficiency for $HCOO^-$ ($EE_{½\ HCOO^-}$) of (55 ± 3)% (Fig. 2B, Table S2). In contrast, Cu GDEs showed low FE_{HCOO^-} values and generated a wide range of products (Fig. 2B, Fig. S5). The FE_{H_2} values were similar for both the bare and modified electrodes, however Cu-SPy displayed significantly lower yields of CO and CO-derived C_2H_4, suggesting that the increase in $HCOO^-$ generation comes at the expense of CO (Fig. 2C).(*38*)

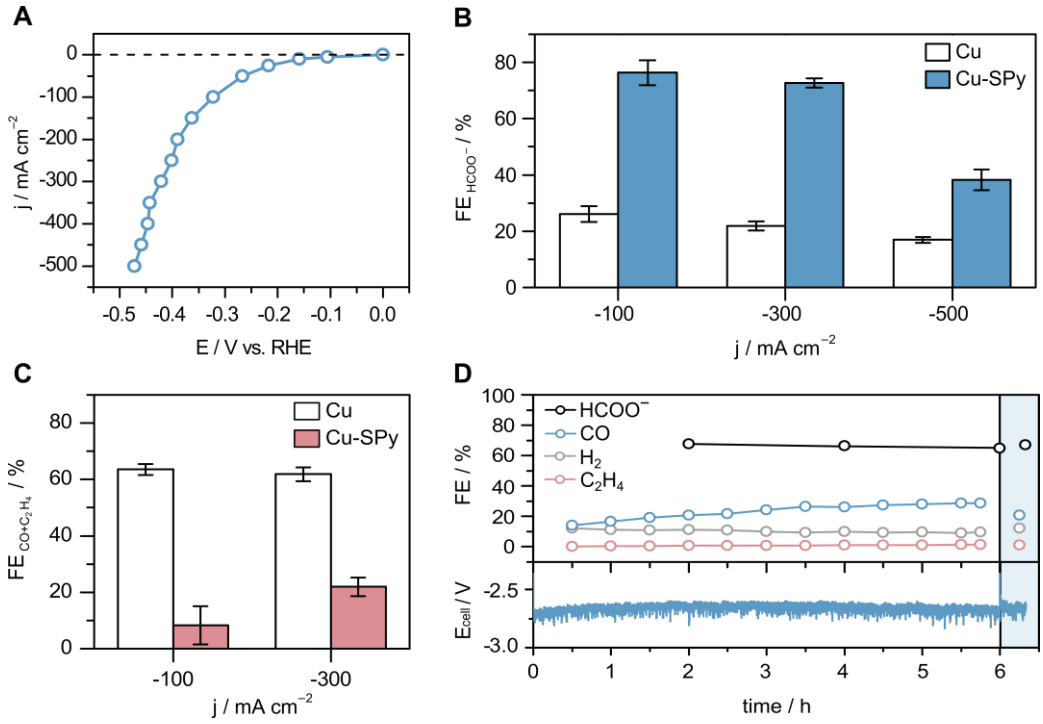

Fig. 2: CO_2 reduction to formate with Cu-SPy electrodes.

(**A**) Current-voltage response (iR-corrected) of a Cu-SPy GDE obtained from chronopotentiometric steps with a 3 min hold time. (**B**) FE_{HCOO^-} values obtained from controlled current electrolysis (CCE) over 1 h with varying current densities for Cu and Cu-SPy electrodes. (**C**) $FE_{CO+C_2H_4}$ values for Cu and Cu-SPy electrodes at different current densities. (**D**) CCE at −300 mA cm^{-2} in a full cell arrangement using a Cu-SPy GDE cathode and a Ni foam anode (no iR correction); the electrolyte solution was replenished after 6 h (shaded blue region represents fresh solution). Error bars represent standard deviation from the mean for triplicate data recorded with fresh electrodes.

At higher current density (−500 mA cm^{-2}) the high formate selectivity was partially lost (FE_{HCOO^-} = (41 ± 4)% after 1h) and the FE_{CO} and $FE_{C_2H_4}$ values increased (Fig. S5). We observed no clear morphological changes following electrolysis that could be responsible for the alteration (Figs. S3 and S6), and the same selectivity trends were observed for purely metallic nanoparticles without air exposure (Cu25-SPy), ruling out oxide retention as a possible factor (Table S3). To determine if SPy desorption was responsible for the alteration, we tracked its presence in the electrolyte solution using UV-Vis spectroscopy (Note S1). At −300 mA cm^{-2} (≈ −0.40 V vs. RHE) < 4% desorption was observed after 1 h, and the presence

of SPy was confirmed using XPS (Fig. S7, Table S4). However, at −500 mA cm^{-2} the amount of SPy desorbed from the GDE increased over the course of electrolysis, which correlated well with a drop in $HCOO^-$ selectivity, and reached roughly 100% desorption after 2 h – at this point the FE_{HCOO^-} was comparable to that of bare Cu (Fig. S8, Table S4). The results established that more cathodic potentials (≈ −0.45 V vs. RHE) give rise to reductive desorption but also verified the essential role SPy plays in altering selectivity.

By altering the flow rate of CO_2, we showed that although higher single-pass carbon efficiency (SPCE) values could be obtained, the highest $HCOO^-$ selectivity was observed with a minimum flow rate of 15 mL min^{-1} (SPCE = 14%) (Fig. S9). We paired the Cu-SPy GDE with a Ni foam anode for water oxidation to drive full-cell CO_2R over the course of 6 h. At −300 mA cm^{-2}, a low and stable full-cell potential (E_{cell}) of −2.7 V was obtained with a steady average FE_{HCOO^-} value of approximately 67%, giving a full-cell energy efficiency for $HCOO^-$ of 31% and a SPCE of 14% (Fig. 2D). No additional SPy was found in solution throughout electrolysis showing that the molecule was stable on the surface (Table S4), and replacement of the electrolyte solution after 6 h showed that the high FE_{HCOO^-} was retained (Fig. 2D), thereby ruling out contributions from solution-dissolved species.

Having established enhanced $HCOO^-$ production with Cu-SPy, we used two thiols with different structural features to help understand the mechanism. We first immobilised thiophenol (SPh), which is structurally similar to SPy but lacks the nitrogen functionality, and conducted CCE experiments under the same conditions as for Cu-SPy. We observed that Cu-SPh GDEs showed comparable $HCOO^-$ selectivity to unmodified Cu electrodes (Table S3) – this suggested that the nitrogen plays a key role in favouring formate production. We next studied the nitrogen contribution by looking into the possibility that reduced pyridine could act as a hydride donor. In highly alkaline conditions at cathodic potentials, dihydropyridine formation is only possible at the 2 or 6 positions of the pyridine.(*39*) Therefore we synthesised

2,6-dimethyl-4-mercaptopyridine (DMSPy), for which these sites are blocked, to see if the selectivity was altered. At −300 mA cm^{-2} we observed similar $HCOO^-$ yields to Cu-SPy, and consequently showed that a pyridine-based hydride mechanism was not possible, in line with previous works (Table S3).(*40*, *41*) These experiments showed that the nitrogen plays an important role but its exact function was unclear. We used DFT calculations to identify possible alterations that could account for the selectivity enhancement.

DFT calculations identified three main pathways involving different reaction intermediates in the formation of CO and $HCOO^-$ (Fig. S12). Two intermediates arising from the first proton-coupled electron transfer produce CO (*OCOH and *OCOH'), and the other intermediate produces $HCOO^-$ (*COOH) (Fig. S13). We performed calculations on each CO_2 reduction and hydrogen evolution pathway with and without the addition of SPy (Figs. S14-S20). There was no alteration to the free energy profile for *H, showing that the molecule does not stabilise hydrogen on the surface; this also supports the experimental results which showed an unaltered FE_{H_2} with Cu-SPy (Fig. S21). Interestingly, the formate pathway showed only minimal free energy changes, as did one of the CO generating pathways (involving *OCOH') (Figs. S22-S23). However, the other CO pathway (involving *OCOH) showed significant increases in the free energies of both the $*CO_2^-$ and *OCOH intermediates in the presence of SPy, thereby blocking this CO_2R pathway (Fig. 3A, Fig. S24). Electron density difference plots identified a destabilising interaction between the N atom of the SPy and the surface-bound intermediate, accounting for this increase in free energy (Fig. 3B). These results show that one of the CO production pathways is thermodynamically inhibited by the presence of SPy. This molecular inhibition mechanism agrees with the described experimental observations that $HCOO^-$ production comes at the expense of CO and C_2H_4 formation. Thus, by preventing CO generation, the surface-bound SPy directs selectivity towards formate.

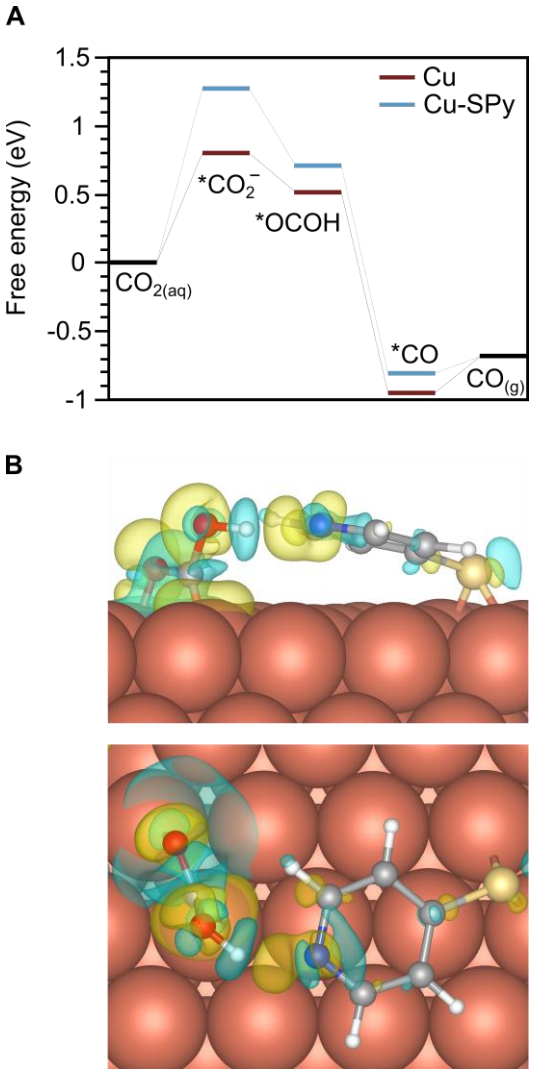

137

Fig. 3: CO inhibition mechanism.

(**A**) Reaction free energy profiles for CO_2 reduction to CO on Cu and Cu-SPy surfaces at −0.4 V vs. RHE. (**B**) Charge density difference plots showing the Cu-SPy interaction with *OCOH, where blue lobes correspond to depletion and yellow lobes correspond to accumulation. Colour code: grey = C, white = H, blue = N, yellow = S, brown = Cu.

138

139 The system presented herein shows that modification of a Cu catalyst with a distinct molecular
140 thiol enhances high-rate CO_2R selectivity by inhibiting production of a specific carbon product.
141 The stability in the gas-fed flow cell at high current densities extends the range of compatible
142 thiols, enabling future catalysts to utilise rational molecular modification to target specific
143 chemical products. Molecular inhibition therefore offers adaptable routes to direct the
144 selectivity of catalytic reactions.

145

References:

1. P. De Luna, C. Hahn, D. Higgins, S. A. Jaffer, T. F. Jaramillo, E. H. Sargent, What would it take for renewably powered electrosynthesis to displace petrochemical processes? *Science*. **364**, eaav3506 (2019).
2. D. Karapinar, C. E. Creissen, J. G. Rivera de la Cruz, M. W. Schreiber, M. Fontecave, Electrochemical CO_2 Reduction to Ethanol with Copper-Based Catalysts. *ACS Energy Lett.* **6**, 694–706 (2021).
3. Y. Y. Birdja, E. Pérez-Gallent, M. C. Figueiredo, A. J. Göttle, F. Calle-Vallejo, M. T. M. Koper, Advances and challenges in understanding the electrocatalytic conversion of carbon dioxide to fuels. *Nat. Energy*. **4**, 732–745 (2019).
4. C. E. Creissen, M. Fontecave, Solar-Driven Electrochemical CO_2 Reduction with Heterogeneous Catalysts. *Adv. Energy Mater.* **11**, 2002652 (2021).
5. S. Nitopi, E. Bertheussen, S. B. Scott, X. Liu, A. K. Engstfeld, S. Horch, B. Seger, I. E. L. Stephens, K. Chan, C. Hahn, J. K. Nørskov, T. F. Jaramillo, I. Chorkendorff, Progress and perspectives of electrochemical CO_2 reduction on copper in aqueous electrolyte. *Chem. Rev.* **119**, 7610–7672 (2019).
6. Y. Hori, I. Takahashi, O. Koga, N. Hoshi, Selective formation of C_2 compounds from electrochemical reduction of CO_2 at a series of copper single crystal electrodes. *J. Phys. Chem. B*. **106**, 15–17 (2002).
7. Z. W. Seh, J. Kibsgaard, C. F. Dickens, I. Chorkendorff, J. K. Nørskov, T. F. Jaramillo, Combining theory and experiment in electrocatalysis: Insights into materials design. *Science*. **355**, eaad4998 (2017).
8. A. A. Peterson, J. K. Nørskov, Activity descriptors for CO_2 electroreduction to methane on transition-metal catalysts. *J. Phys. Chem. Lett.* **3**, 251–258 (2012).
9. T. K. Todorova, M. W. Schreiber, M. Fontecave, Mechanistic Understanding of CO_2 Reduction Reaction (CO_2RR) Toward Multicarbon Products by Heterogeneous

Copper-Based Catalysts. *ACS Catal.* **10**, 1754–1768 (2020).

10. P. De Luna, R. Quintero-Bermudez, C. T. DInh, M. B. Ross, O. S. Bushuyev, P. Todorović, T. Regier, S. O. Kelley, P. Yang, E. H. Sargent, Catalyst electro-redeposition controls morphology and oxidation state for selective carbon dioxide reduction. *Nat. Catal.* **1**, 103–110 (2018).

11. A. Loiudice, P. Lobaccaro, E. A. Kamali, T. Thao, B. H. Huang, J. W. Ager, R. Buonsanti, Tailoring Copper Nanocrystals towards C_2 Products in Electrochemical CO_2 Reduction. *Angew. Chem. Int. Ed.* **55**, 5789–5792 (2016).

12. K. Jiang, R. B. Sandberg, A. J. Akey, X. Liu, D. C. Bell, J. K. Nørskov, K. Chan, H. Wang, Metal ion cycling of Cu foil for selective C-C coupling in electrochemical CO_2 reduction. *Nat. Catal.* **1**, 111–119 (2018).

13. Y. Wang, Z. Wang, C. T. Dinh, J. Li, A. Ozden, M. Golam Kibria, A. Seifitokaldani, C. S. Tan, C. M. Gabardo, M. Luo, H. Zhou, F. Li, Y. Lum, C. McCallum, Y. Xu, M. Liu, A. Proppe, A. Johnston, P. Todorovic, T. T. Zhuang, D. Sinton, S. O. Kelley, E. H. Sargent, Catalyst synthesis under CO_2 electroreduction favours faceting and promotes renewable fuels electrosynthesis. *Nat. Catal.* **3**, 98–106 (2020).

14. R. G. Mariano, K. McKelvey, H. S. White, M. W. Kanan, Selective increase in CO_2 electroreduction activity at grain-boundary surface terminations. *Science*. **358**, 1187–1192 (2017).

15. J. Vavra, T. H. Shen, D. Stoian, V. Tileli, R. Buonsanti, Real-time Monitoring Reveals Dissolution/Redeposition Mechanism in Copper Nanocatalysts during the Initial Stages of the CO_2 Reduction Reaction. *Angew. Chem. Int. Ed.* **60**, 1347–1354 (2021).

16. R. M. Arán-Ais, R. Rizo, P. Grosse, G. Algara-Siller, K. Dembélé, M. Plodinec, T. Lunkenbein, S. W. Chee, B. R. Cuenya, Imaging electrochemically synthesized Cu_2O cubes and their morphological evolution under conditions relevant to CO_2 electroreduction. *Nat. Commun.* **11**, 3489 (2020).

17. J. Huang, N. Hörmann, E. Oveisi, A. Loiudice, G. L. De Gregorio, O. Andreussi, N. Marzari, R. Buonsanti, Potential-induced nanoclustering of metallic catalysts during

electrochemical CO_2 reduction. *Nat. Commun.* **9**, 1–9 (2018).

18. A. Wagner, C. D. Sahm, E. Reisner, Towards molecular understanding of local chemical environment effects in electro- and photocatalytic CO_2 reduction. *Nat. Catal.* **3**, 775–786 (2020).

19. D. H. Nam, P. De Luna, A. Rosas-Hernández, A. Thevenon, F. Li, T. Agapie, J. C. Peters, O. Shekhah, M. Eddaoudi, E. H. Sargent, Molecular enhancement of heterogeneous CO_2 reduction. *Nat. Mater.* **19**, 266–276 (2020).

20. Y. Fang, J. C. Flake, Electrochemical Reduction of CO_2 at Functionalized Au Electrodes. *J. Am. Chem. Soc.* **139**, 3399–3405 (2017).

21. F. Li, Y. C. Li, Z. Wang, J. Li, D. H. Nam, Y. Lum, M. Luo, X. Wang, A. Ozden, S. F. Hung, B. Chen, Y. Wang, J. Wicks, Y. Xu, Y. Li, C. M. Gabardo, C. T. Dinh, Y. Wang, T. T. Zhuang, D. Sinton, E. H. Sargent, Cooperative CO_2-to-ethanol conversion via enriched intermediates at molecule–metal catalyst interfaces. *Nat. Catal.* **3**, 75–82 (2020).

22. Z. Han, R. Kortlever, H. Y. Chen, J. C. Peters, T. Agapie, CO_2 Reduction Selective for $C_{\geq 2}$ Products on Polycrystalline Copper with N-Substituted Pyridinium Additives. *ACS Cent. Sci.* **3**, 853–859 (2017).

23. F. Li, A. Thevenon, A. Rosas-Hernández, Z. Wang, Y. Li, C. M. Gabardo, A. Ozden, C. T. Dinh, J. Li, Y. Wang, J. P. Edwards, Y. Xu, C. McCallum, L. Tao, Z. Q. Liang, M. Luo, X. Wang, H. Li, C. P. O'Brien, C. S. Tan, D. H. Nam, R. Quintero-Bermudez, T. T. Zhuang, Y. C. Li, Z. Han, R. D. Britt, D. Sinton, T. Agapie, J. C. Peters, E. H. Sargent, Molecular tuning of CO_2-to-ethylene conversion. *Nature*. **577**, 509–513 (2020).

24. T. T. H. Hoang, S. Ma, J. I. Gold, P. J. A. Kenis, A. A. Gewirth, Nanoporous Copper Films by Additive-Controlled Electrodeposition: CO_2 Reduction Catalysis. *ACS Catal.* **7**, 3313–3321 (2017).

25. M. S. Xie, B. Y. Xia, Y. Li, Y. Yan, Y. Yang, Q. Sun, S. H. Chan, A. Fisher, X. Wang, Amino acid modified copper electrodes for the enhanced selective electroreduction of

carbon dioxide towards hydrocarbons. *Energy Environ. Sci.* **9**, 1687–1695 (2016).

26. X. Chen, J. Chen, N. M. Alghoraibi, D. A. Henckel, R. Zhang, U. O. Nwabara, K. E. Madsen, P. J. A. Kenis, S. C. Zimmerman, A. A. Gewirth, Electrochemical CO_2-to-ethylene conversion on polyamine-incorporated Cu electrodes. *Nat. Catal.* **4**, 20–27 (2021).

27. S. Ahn, K. Klyukin, R. J. Wakeham, J. A. Rudd, A. R. Lewis, S. Alexander, F. Carla, V. Alexandrov, E. Andreoli, Poly-Amide Modified Copper Foam Electrodes for Enhanced Electrochemical Reduction of Carbon Dioxide. *ACS Catal.* **8**, 4132–4142 (2018).

28. J. R. Pankhurst, P. Iyengar, A. Loiudice, M. Mensi, R. Buonsanti, Metal-ligand bond strength determines the fate of organic ligands on the catalyst surface during the electrochemical CO_2 reduction reaction. *Chem. Sci.* **11**, 9296–9302 (2020).

29. J. C. Love, L. A. Estroff, J. K. Kriebel, R. G. Nuzzo, G. M. Whitesides, Self-assembled monolayers of thiolates on metals as a form of nanotechnology. *Chem. Rev.* **105**, 1103–1169 (2005).

30. D. Wakerley, S. Lamaison, F. Ozanam, N. Menguy, D. Mercier, P. Marcus, M. Fontecave, V. Mougel, Bio-inspired hydrophobicity promotes CO_2 reduction on a Cu surface. *Nat. Mater.* **18**, 1222–1227 (2019).

31. D. Kim, S. Yu, F. Zheng, I. Roh, Y. Li, S. Louisia, Z. Qi, G. A. Somorjai, H. Frei, L. W. Wang, P. Yang, Selective CO_2 electrocatalysis at the pseudocapacitive nanoparticle/ordered-ligand interlayer. *Nat. Energy*. **5**, 1032–1042 (2020).

32. F. P. García de Arquer, C. T. Dinh, A. Ozden, J. Wicks, C. McCallum, A. R. Kirmani, D. H. Nam, C. Gabardo, A. Seifitokaldani, X. Wang, Y. C. Li, F. Li, J. Edwards, L. J. Richter, S. J. Thorpe, D. Sinton, E. H. Sargent, CO_2 electrolysis to multicarbon products at activities greater than 1 A cm^{-2}. *Science*. **367**, 661–666 (2020).

33. M. Zhong, K. Tran, Y. Min, C. Wang, Z. Wang, C. T. Dinh, P. De Luna, Z. Yu, A. S. Rasouli, P. Brodersen, S. Sun, O. Voznyy, C. S. Tan, M. Askerka, F. Che, M. Liu, A. Seifitokaldani, Y. Pang, S. C. Lo, A. Ip, Z. Ulissi, E. H. Sargent, Accelerated discovery

of CO_2 electrocatalysts using active machine learning. *Nature*. **581**, 178–183 (2020).

34. S. Herrera, F. Tasca, F. J. Williams, E. J. Calvo, P. Carro, R. C. Salvarezza, Surface Structure of 4-Mercaptopyridine on Au(111): A New Dense Phase. *Langmuir*. **33**, 9565–9572 (2017).

35. D. G. Castner, K. Hinds, D. W. Grainger, X-ray photoelectron spectroscopy sulfur 2p study of organic thiol and bisulfide binding interactions with gold surfaces. *Langmuir*. **12**, 5083–5086 (1996).

36. Y. Wang, J. Im, J. W. Soares, D. M. Steeves, J. E. Whitten, Thiol Adsorption on and Reduction of Copper Oxide Particles and Surfaces. *Langmuir*. **32**, 3848–3857 (2016).

37. A. Thevenon, A. Rosas-Hernández, J. C. Peters, T. Agapie, In-Situ Nanostructuring and Stabilization of Polycrystalline Copper by an Organic Salt Additive Promotes Electrocatalytic CO2 Reduction to Ethylene. *Angew. Chem. Int. Ed.* **58**, 16952–16958 (2019).

38. J. H. Montoya, C. Shi, K. Chan, J. K. Nørskov, Theoretical insights into a CO dimerization mechanism in CO_2 electroreduction. *J. Phys. Chem. Lett.* **6**, 2032–2037 (2015).

39. J. A. Keith, E. A. Carter, Electrochemical reactivities of pyridinium in solution: Consequences for CO_2 reduction mechanisms. *Chem. Sci.* **4**, 1490–1496 (2013).

40. C. Costentin, J. M. Savéant, C. Tard, Catalysis of CO_2 Electrochemical Reduction by Protonated Pyridine and Similar Molecules. Useful Lessons from a Methodological Misadventure. *ACS Energy Lett.* **3**, 695–703 (2018).

41. M. Dunwell, Y. Yan, B. Xu, In Situ Infrared Spectroscopic Investigations of Pyridine-Mediated CO_2 Reduction on Pt Electrocatalysts. *ACS Catal.* **7**, 5410–5419 (2017).

Acknowledgements:

We thank Arnaud Etcheberry, Mathieu Fregnaux, and Muriel Bouttemy for XPS measurements, and Françoise Pillier for SEM analysis. **Funding:** This work was supported financially by funding from Total Research & Technology Feluy. This work was granted access to the HPC/AI resources of TGCC under the allocation 2020-A0090811911 made by GENCI.

Author Contributions: C.E.C. and M.F. conceived the research. C.E.C. performed electrocatalysis, synthesis, and characterisation. J.G.R.C. conducted DFT calculations. D.K. carried out IR measurements. D.T. conducted TEM measurements. All authors analysed the data. C.E.C. wrote the manuscript. M.F., J.G.R.C., D.K., and M.S. contributed to discussions and manuscript preparation. M.F. supervised the work. **Competing Interests:** A provisional European patent application for this work (EP21315179.8) was filed on the 24th of September 2021 in the joint names of Total SE and Collège de France. **Data and Materials Availability:** The datasets generated during and/or analysed during the current study are available from the corresponding author on reasonable request.

Supplementary Materials:

Materials and Methods

Computational Methods and Models

Supplementary Figures and Notes

Supplementary Tables S1 – S6

Supplementary References

Correspondence and requests for materials should be addressed to

marc.fontecave@college-de-france.fr